Analysis and Compensation of the System Time Delay in an MMC System

Chuyang Wang, Lan Xiao, *Member, IEEE*, Huijie Jiang, and Tingting Cai

***Abstract*—The system time delay (STD) is typically neglected in the design of a modular multilevel converter system. However, the STD can cause different types of deteriorations, including a decrease in system stability, a weakening of the steady-state performance, and a deceleration of the transient response when the load changes. This study first provides the generation mechanism and classification of the system time delay. Then, a linear model is developed to form the basis of the analysis for the system time delay. Subsequently, an analytical method is used to provide an accurate description of the relation between the STD and corresponding deteriorations. Based on the analysis, the optimal design methods of the system controller parameters are proposed to effectively mitigate these deteriorations. Finally, the deteriorations caused by the STD and efficiency of the optimal design methods are demonstrated via experiments.**

***Index Terms*—Modular multilevel converter, optimal design methods, steady-state performance, system stability, system time delay, transient response.**

I. Introduction

THE modular multilevel converter (MMC) changes alternating voltage into direct voltage or vice versa, and has been widely used in the fields of high-voltage direct current transmission (HVDC), active power filter, static var generators, etc. To ensure the stable operation of the MMC system, linear models of MMC systems have been presented in [1]–[5], and the corresponding control strategies have been developed in [6]. However, when variables in the primary circuit, such as the arm currents and alternating voltages, are required in the control system, the system time delay (STD) exists, leading to an inaccuracy in the linear model, a decrease in the reliability of the control strategy and deteriorations in the system performance for an MMC system.

Currently, the effect of the STD is rarely considered in MMC systems; however, it has been considered in two-level converters in several publications [7]. The authors in [8]–[13] considered the STD and determined that it could decrease system stability; however, the studies did not provide an applicable method to increase the stability. The authors in [14]–[20] used a controller based on a predictive current observer to compensate for the STD; however, the observers were sensitive to variations in the parameters, which might cause additional estimation or prediction errors and were not applicable for MMC systems. The authors in [21]–[24] decreased the STD using a high-speed digital chip and compacting control codes; however, this method could not substantially decrease the STD effect. The authors in [25]–[30] used state equations to determine the system's next state to decrease the STD; however, the MMC is a complex system and its state equations are difficult to obtain. A method based on a Smith predictor was proposed to compensate for the STD in [31], but the predictor was difficult to construct because it was based on a complex analogue circuit. Wang *et al.* [32] artificially increased the value of the STD to improve the system stability, but was only applicable for a two-level converter with an LCL filter. Chen *et al.* [33] introduces a lead-lag network into the control system to compensate for the STD. However, the parameters in the lead-lag network are complex to be determined.

These previous studies demonstrate that the STD decreases the system performance and should thus be considered and compensated for in the MMC system. Furthermore, the MMC system analyzed in this paper has a relatively low number of submodules, and thus uses the modulation method of carrier phase-shift pulse-width modulation (CPS-PWM) to generate switch drives. The main contributions of this paper in comparison with the previous works are summarized below.

First, few previous studies have considered the STD in MMC systems. This paper studies the generation mechanism of the STD in such systems and deduces the corresponding effects, providing the theoretical basis of STD compensation methods.

Second, this paper establishes a simplified linear model of MMC systems to quantitatively determine the effects of the STDs, which include a decrease in the system stability, a reduction in the system steady-state performance, and an aggravation in the system transient response.

Third, based on the analysis of the STD effects, this paper proposes optimal design methods of the system controller parameters to mitigate the deteriorations caused by the STD, which greatly improves the system working performance and are applicable to most MMC systems.

The remainder of this paper is organized as follows: Section II presents the generation mechanism and classifica-

Manuscript received August 17, 2017; revised November 28, 2017; accepted January 2, 2018. Date of publication January 10, 2018; date of current version August 7, 2018. This work was supported in part by the National Natural Science Foundation of China under Grant 61673210, and in part by the Jiangsu Qing Lan Project and the Jiangsu Province University Outstanding Science and Technology Innovation Team Project. Recommended for publication by Associate Editor G. Konstantinou. *(Corresponding author: Lan Xiao.)*

The authors are with the School of Engineering, Department of Electrical Engineering, Nanjing University of Aeronautics and Astronautics, Nanjing 211106, China (e-mail: 792246001@qq.com; xiaolan@nuaa.edu.cn; 939255652@qq.com; 996444688@qq.com).

Color versions of one or more of the figures in this paper are available online at http://ieeexplore.ieee.org.

Digital Object Identifier 10.1109/TPEL.2018.2791573

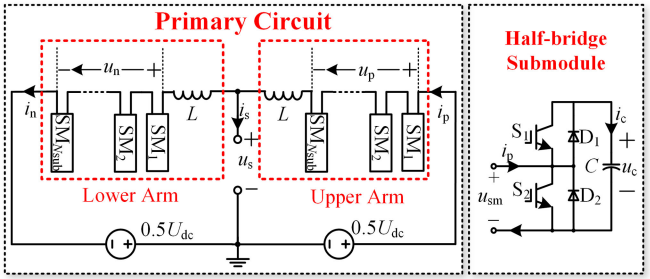

Fig. 1. Primary topology of a single-phase MMC system.

tion of STDs in MMC systems. Section III establishes a linear model for MMC systems, and presents a quantitative analysis of the STD effects on the system. Section IV proposes optimal design methods to improve the system performance and to mitigate the deteriorations caused by the STD. Experimental results are used to confirm the theoretical analysis and design methods in Section VI, and concluding remarks are provided in Section VII.

II. Generation Mechanism and Classification of the STD

The STD in MMC systems is primarily generated by the sampling circuit, analog–digital (AD) conversion, calculation process in the digital signal processor (DSP) and pulse width modulation (PWM) process in field programmable gate array (FPGA), making the digital variables in the control system different from the analogue variables in the primary circuit. To provide a simplified analysis of the STD effect on an MMC system, this paper considers a single-phase MMC system instead of a three-phase one, with the primary topology of the system shown in Fig. 1.

In Fig. 1, u_p and u_n are the upper and lower arm voltages, respectively. i_p and i_n are the upper and lower arm currents, respectively. u_s is the alternating voltage, i_s is the alternating current, L is the inductor, and $N_{\rm sub}$ is the submodule number in each arm. The system works as an inverter, and its direct voltage $U_{\rm dc}$ is set to a constant value. The submodule's simplest topology is a half bridge, where C is the submodule capacitor, and S_1 and S_2 are the up and down switches, respectively. Therefore, the submodule has two types of operating modes: the inserted mode, where S_1 is on and S_2 is off, and the bypassed mode, where S_1 is off and S_2 is on. Losses and other parasitic parameters are neglected in the analysis. The fundamental frequency of u_s and i_s is f_0, which is typically set to 50 Hz. The switching frequency is f_s, and the corresponding switching period is T_s. The sampling and control frequencies are both $f_{\rm sa}$, and the corresponding period is $T_{\rm sa}$. The MMC in this study uses CPS-PWM method as its modulation strategy. $f_{\rm sa}$ is typically set as equal to or double the value of f_s, which is similar to that in a two-level converter.

Based on the characteristic of the MMC topology and corresponding variables in the primary circuit, three types of STDs are present in the control system, namely, the STD related to the capacitor voltages u_c, the STDs related to the ac variables i_p, i_n, and u_s (STD-AC) and the STD related to $U_{\rm dc}$. This paper focuses the studies on the STD-AC, and the generation mechanism of the STD-AC is shown in Fig. 2.

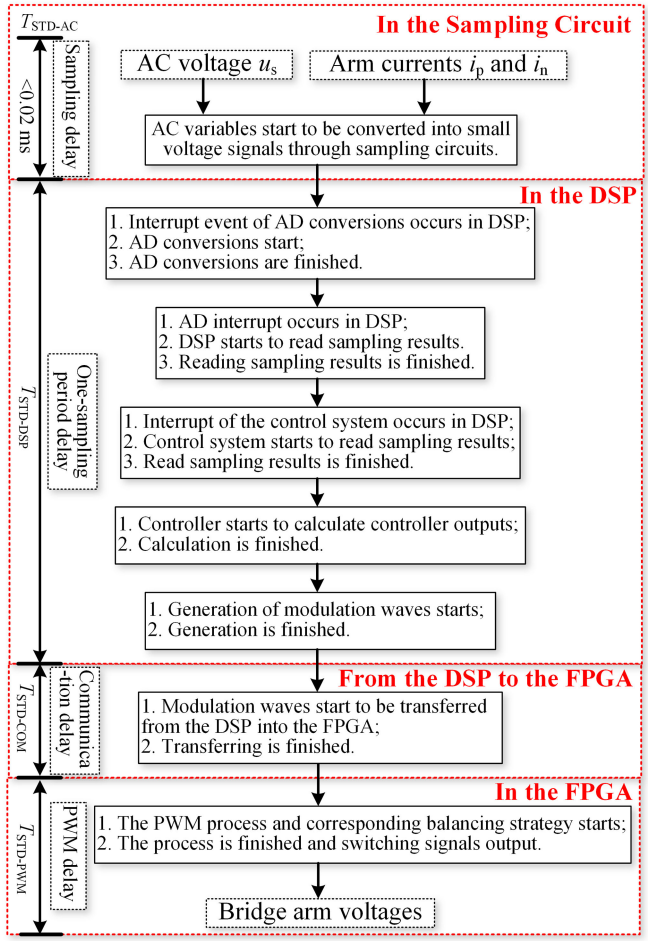

Fig. 2. Generation mechanism of the STD-AC in the control system.

In Fig. 2, the STD-AC contains four components:

1) Sampling delay, which is primarily generated by the hardware in the system, including the voltage and current sensors, filters with resistors and capacitors, and the operational amplifiers in the sampling circuits. However, this delay is typically smaller than 0.02 ms and can thus be neglected in the MMC system.
2) One-sampling period delay, which is generated by the signal processing in the DSP (STD-DSP) with a corresponding value of $T_{\rm STD\text{-}DSP}$. $T_{\rm STD\text{-}DSP}$ is the same in i_p, i_n, and u_s because they have similar generation mechanisms.
3) Communication delay, which is generated by the transmission process of the modulation waves (STD-COM) with a corresponding value of $T_{\rm STD\text{-}COM}$. An overall system uses a 16-bit or 32-bit asynchronous bus to transmit the modulation waves from the DSP to the FPGA in the main control, and then generates the switch drives. Therefore, the communication delay is small. However, a distributed system in certain applications uses SPI, CAN,

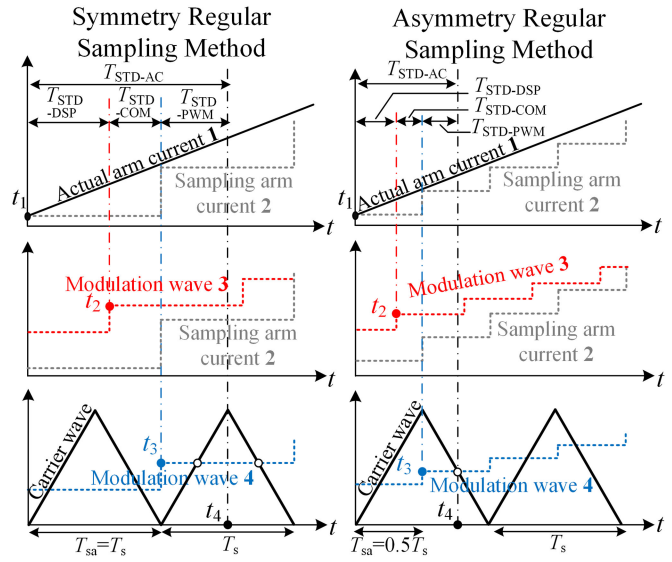

Fig. 3. Quantitative relations between $T_{\text{STD-AC}}$, $T_{\text{STD-DSP}}$, $T_{\text{STD-COM}}$, and $T_{\text{STD-PWM}}$.

Ethercat, or other communication protocols to transmit the modulation waves from the DSP in the main control to the submodules, making $T_{\text{STD-COM}}$ greater than 0.2 ms. In such situations, $T_{\text{STD-COM}}$ cannot be neglected in the STD-AC.

4) PWM delay, which is generated by the PWM process in the FPGA (STD-PWM) with a corresponding value of $T_{\text{STD-PWM}}$.

Furthermore, the quantitative relations between T_s, T_{sa}, $T_{\text{STD-AC}}$, $T_{\text{STD-DSP}}$, $T_{\text{STD-COM}}$, and $T_{\text{STD-PWM}}$ are shown in Fig. 3, where the sampling process of the arm current is used as an example.

In Fig. 3, two methods are used in the sampling process: the symmetry regular sampling (SRS) method and asymmetry regular sampling (ARS) method. In the SRS mode, the arm currents are sampled once but the modulation wave is compared with the carrier wave twice during one switching period. In the ARS mode, the arm currents are sampled twice and the modulation wave is compared with the carrier wave twice as well during one switching period. Based on these two sampling methods, actual arm current 1 is sampled at time t_1 to obtain sampling arm current 2 in the DSP. Modulation wave 3 is then determined at time t_2, and the corresponding value 4 is subsequently updated in the FPGA at time t_3. The modulation wave is eventually compared with carrier waves to generate the switch drives at time t_4. The times from t_1 to t_2, from t_2 to t_3, from t_3 to t_4, and from t_1 to t_4 are defined as $T_{\text{STD-DSP}}$, $T_{\text{STD-COM}}$, $T_{\text{STD-PWM}}$, and $T_{\text{STD-AC}}$, respectively, and the corresponding values of $T_{\text{STD-DSP}}$, $T_{\text{STD-PWM}}$, $T_{\text{STD-COM}}$, and $T_{\text{STD-AC}}$ that were determined based on Fig. 3 are shown in Table I, where η is a coefficient with values ranging from 0 to 1. According to Table I, $T_{\text{STD-AC}}$ is smaller than 0.1 ms in a two-level converter because T_s is smaller than 0.1 ms and $T_{\text{STD-COM}}$ is very small. Therefore, $T_{\text{STD-AC}}$ has a relative small effect on its performance. However, f_s can reach to a low value in the MMC system, and the corresponding $T_{\text{STD-AC}}$ can have a greater value (0.5 ms or more) at the same time, causing the system performance to deteriorate considerably. Thus, the effects of the STD-AC on the MMC system are extremely important, and are thus quantitatively analyzed below.

TABLE I
VALUES OF $T_{\text{STD-DSP}}$, $T_{\text{STD-PWM}}$, AND $T_{\text{STD-AC}}$

	$T_{\text{STD-DSP}}$	$T_{\text{STD-PWM}}$	$T_{\text{STD-COM}}$	$T_{\text{STD-AC}}$
SRS mode	ηT_s	$0.5T_s$	Overall: Neglected Distributed: ≥ 0.2 ms	$(\eta+0.5)T_s$ $(\eta+0.5)T_s+T_{\text{STD-COM}}$
ARS mode	$0.5\eta T_s$	$0.25T_s$	Overall: Neglected Distributed: ≥ 0.2 ms	$(0.5\eta+0.25)Ts$ $(0.5\eta+0.25)Ts+T_{\text{STD-COM}}$

III. EFFECTS OF THE STD-AC ON THE MMC SYSTEM

A. Establishment of the System Linear Model Under the Effects of the STD-AC

To enable a precise analysis of the STD-AC effects on the MMC system, the linear model of a single-phase MMC system should be developed. Based on the topology in Fig. 1, the state equations of the MMC system are as follows:

$$\begin{cases} u_s+\sum_{i=1}^{N_{\text{sub}}}\varepsilon_{i\_p}u_{\text{ci\_}p}+L\dfrac{di_p}{dt}=\dfrac{U_{\text{dc}}}{2} \\ -u_s+\sum_{i=1}^{N_{\text{sub}}}\varepsilon_{i\_n}u_{\text{ci\_}n}+L\dfrac{di_n}{dt}=\dfrac{U_{\text{dc}}}{2} \\ i_s=i_p-i_n \\ 2i_z=i_p+i_n \end{cases} \tag{1}$$

where ε_{i_p} and ε_{i_n} are the states of S_1 of the submodules in the upper and lower arms, respectively, $u_{\text{ci\_}p}$ and $u_{\text{ci\_}n}$ are the capacitor voltages of the submodules in the upper and lower arms, respectively, and i_z is the circulating current. Equation (1) is redefined as (2) because i_z and i_s are the variables that must be directly controlled

$$\begin{cases} L\dfrac{di_s}{dt}+2u_s=-u_p+u_n \\ \quad=-\left(\sum_{i=1}^{N_{\text{sub}}}\varepsilon_{i\_p}u_{\text{ci\_}p}-\sum_{i=1}^{N_{\text{sub}}}\varepsilon_{i\_n}u_{\text{ci\_}n}\right) \\ L\dfrac{d2i_z}{dt}=U_{\text{dc}}-(u_p+u_n)=U_{\text{dc}} \\ \quad-\left(\sum_{i=1}^{N_{\text{sub}}}\varepsilon_{i\_p}u_{\text{ci\_}p}+\sum_{i=1}^{N_{\text{sub}}}\varepsilon_{i\_n}u_{\text{ci\_}n}\right) \end{cases} \tag{2}$$

ε_{i_p} and ε_{i_n} make certain variables in (2) contain high-frequency components; thus, an average state-space method should be used to omit these components, and (2) can be

redefined as (3) at low frequencies

$$\begin{cases} L\dfrac{d\langle i_s\rangle_{T_s}}{dt}+2\langle u_s\rangle_{T_s}=-\langle u_p\rangle_{T_s}+\langle u_n\rangle_{T_s} \\ =-\left(\sum_{i=1}^{N_{\rm sub}}\langle\varepsilon_{i\_p}u_{{\rm ci}\_p}\rangle_{T_s}-\sum_{i=1}^{N_{\rm sub}}\langle\varepsilon_{i\_n}u_{{\rm ci}\_n}\rangle_{T_s}\right) \\ L\dfrac{d2\langle i_z\rangle_{T_s}}{dt}=U_{dc}-(\langle u_p\rangle_{T_s}+\langle u_n\rangle_{T_s}) \\ =U_{\rm dc}-\left(\sum_{i=1}^{N_{\rm sub}}\langle\varepsilon_{i\_p}u_{{\rm ci}\_p}\rangle_{T_s}+\sum_{i=1}^{N_{\rm sub}}\langle\varepsilon_{i\_n}u_{{\rm ci}\_n}\rangle_{T_s}\right) \end{cases} \tag{3}$$

However, (3) is difficult to analyse because the items in (3) include numerous variables, causing the system to be ultra-high order. Therefore, three assumptions are provided to simplify (3):

1) The MMC works as an inverter, and $U_{\rm dc}$ is approximately constant.
2) The capacitor voltages u_c of the different submodules in the upper arm are set to the same variables, which contains dc bias $U_{\rm dc}/N_{\rm sub}$ and alternating component $\sim U_{\rm cp}$. Alternatively, the capacitor voltages u_c of the different submodules in the lower arm are set to the same variables as well, which contains dc bias $U_{\rm dc}/N_{\rm sub}$ and alternating component $\sim U_{\rm cn}$.
3) $<\varepsilon_{1\_p}>_{\rm Ts}, <\varepsilon_{2\_p}>_{\rm Ts}\cdots<\varepsilon_{N{\rm sub}\_p}>_{\rm Ts}$ are set to the same variables such that they can be represented by the same item $<s_p>_{\rm Ts}$. Alternatively, $<\varepsilon_{1\_n}>_{\rm Ts}$, $<\varepsilon_{2\_n}>_{\rm Ts}\cdots<\varepsilon_{N{\rm sub}\_n}>_{\rm Ts}$ can be represented by $<s_n>_{\rm Ts}$.

Based on these assumptions, the average arm voltages $<u_p>_{\rm Ts}$ and $<u_n>_{\rm Ts}$ can be redefined as

$$\begin{cases} \langle u_p\rangle_{T_s}=\sum_{i=1}^{N_{\rm sub}}\langle\varepsilon_{pi}u_{c\_{\rm pi}}\rangle_{T_s}\approx\left(\dfrac{U_{\rm dc}}{N_{\rm sub}}+\tilde{U}_{\rm cp}\right) \\ \quad\times\sum_{i=1}^{N_{\rm sub}}\langle\varepsilon_{pi}\rangle_{T_s} \\ \approx\left(\dfrac{U_{\rm dc}}{N_{\rm sub}}+\tilde{U}_{\rm cp}\right)N_{\rm sub}\langle s_p\rangle_{T_s}=(U_{\rm dc}+N_{\rm sub}\tilde{U}_{\rm cp})\langle s_p\rangle_{T_s} \\ \langle u_n\rangle_{T_s}=\sum_{i=1}^{N_{\rm sub}}\langle\varepsilon_{ni}u_{c\_{\rm ni}}\rangle_{T_s}\approx(U_{\rm dc}+N_{\rm sub}\tilde{U}_{\rm cn})\langle s_n\rangle_{T_s} \end{cases} \tag{4}$$

Therefore, (3) can be redefined as (5) when the small and large signals in (3) are separated

$$\begin{cases} L\dfrac{d}{dt}(\tilde{I}_s+\hat{i}_s)+2(\tilde{U}_s+\hat{u}_s)=-(U_{\rm dc}+N_{\rm sub}\tilde{U}_{\rm cp})(\tilde{S}_p+\hat{s}_p) \\ +(U_{\rm dc}+N_{\rm sub}\tilde{U}_{\rm cn})(\tilde{S}_n+\hat{s}_n) \\ L\dfrac{d}{dt}2(\tilde{I}_z+\hat{i}_z)=U_{\rm dc}-(U_{\rm dc}+N_{\rm sub}\tilde{U}_{\rm cp})(\tilde{S}_p+\hat{s}_p) \\ -(U_{\rm dc}+N_{\rm sub}\tilde{U}_{\rm cn})(\tilde{S}_n+\hat{s}_n) \end{cases} \tag{5}$$

where $\tilde{I}_s, \tilde{I}_z, \tilde{U}_s, \tilde{U}_{\rm cp}$, and $\tilde{U}_{\rm cn}$ are the large signals. Based on (5), the large and small signal equations can be both determined.

$$\begin{cases} L\dfrac{d\tilde{I}_s}{dt}+2\tilde{U}_s=-(U_{\rm dc}+N_{\rm sub}\tilde{U}_{\rm cp})\tilde{S}_p \\ +(U_{\rm dc}+N_{\rm sub}\tilde{U}_{\rm cn})\tilde{S}_n \\ L\dfrac{d(2\tilde{I}_z)}{dt}-U_{\rm dc}=-(U_{\rm dc}+N_{\rm sub}\tilde{U}_{\rm cp})\tilde{S}_p \\ -(U_{\rm dc}+N_{\rm sub}\tilde{U}_{\rm cn})\tilde{S}_n \end{cases}$$

$$\begin{cases} L\dfrac{d\hat{i}_s}{dt}=-2\hat{u}_s-(U_{\rm dc}+N_{\rm sub}\tilde{U}_{\rm cp})\hat{s}_p \\ +(U_{\rm dc}+N_{\rm sub}\tilde{U}_{\rm cn})\hat{s}_n=\hat{u}_1 \\ L\dfrac{d(2\hat{i}_z)}{dt}=-(U_{\rm dc}+N_{\rm sub}\tilde{U}_{\rm cp})\hat{s}_p \\ -(U_{\rm dc}+N_{\rm sub}\tilde{U}_{\rm cn})\hat{s}_n=2\hat{u}_2 \end{cases} \tag{6}$$

where $\hat{u}_1$ and $\hat{u}_2$ are new variables that are linearly related to the small signals of i_s and i_z, respectively. Thus, i_s and i_z can be directly controlled when $\hat{u}_1$ and $2\hat{u}_2$ are defined as the controller outputs. Furthermore, (7) can be obtained based on (6):

$$\begin{cases} (U_{\rm dc}+N_{\rm sub}\tilde{U}_{\rm cp})\tilde{S}_p=\dfrac{1}{2}U_{\rm dc}-\tilde{U}_s-L\dfrac{d\tilde{I}_p}{dt}\approx\dfrac{1}{2}U_{\rm dc}-\tilde{U}_s \\ (U_{\rm dc}+N_{\rm sub}\tilde{U}_{\rm cn})\tilde{S}_n=\dfrac{1}{2}U_{\rm dc}+\tilde{U}_s-L\dfrac{d\tilde{I}_n}{dt}\approx\dfrac{1}{2}U_{\rm dc}+\tilde{U}_s \end{cases}$$

$$\begin{cases} (U_{\rm dc}+N_{\rm sub}\tilde{U}_{\rm cp})\hat{s}_p=-\hat{u}_s-\dfrac{\hat{u}_1+2\hat{u}_2}{2} \\ (U_{\rm dc}+N_{\rm sub}\tilde{U}_{\rm cn})\hat{s}_n=\hat{u}_s+\dfrac{\hat{u}_1-2\hat{u}_2}{2} \end{cases} \tag{7}$$

Because only $<u_p>_{\rm Ts}$ and $<u_n>_{\rm Ts}$ can be used as modulation waves to generate the switch drives but $\hat{u}_1$ and $\hat{u}_2$ do not have the same characteristics, the relations between $\hat{u}_1, \hat{u}_2, <u_p>_{\rm Ts}$, and $<u_n>_{\rm Ts}$ should be determined, which can be described as (8) based on (4) and (7)

$$\begin{cases} \langle u_p\rangle_{T_s}=(U_{\rm dc}+N_{\rm sub}\tilde{U}_{\rm cp})\langle s_p\rangle_{T_s}=(U_{\rm dc}+N_{\rm sub}\tilde{U}_{\rm cp})\tilde{S}_p \\ +(U_{\rm dc}+N_{\rm sub}\tilde{U}_{\rm cp})\hat{s}_p\approx\dfrac{1}{2}U_{\rm dc}-\langle u_s\rangle_{T_s}-\dfrac{\hat{u}_1+2\hat{u}_2}{2} \\ \langle u_n\rangle_{T_s}=(U_{\rm dc}+N_{\rm sub}\tilde{U}_{\rm cn})\langle s_n\rangle_{T_s}=(U_{\rm dc}+N_{\rm sub}\tilde{U}_{\rm cn})\tilde{S}_n \\ +(U_{\rm dc}+N_{\rm sub}\tilde{U}_{\rm cn})\hat{s}_n\approx\dfrac{1}{2}U_{\rm dc}+\langle u_s\rangle_{T_s}+\dfrac{\hat{u}_1-2\hat{u}_2}{2} \end{cases} \tag{8}$$

Therefore, the control strategy of a single-phase MMC system is shown in Fig. 4 based on (8).

In Fig. 4, proportional-integral (PI) controllers are used in the system, including an outer loop controller for u_s, an inner loop controller for i_s and a circulating current controller for i_z. The references of the inner loop, outer loop and circulating current

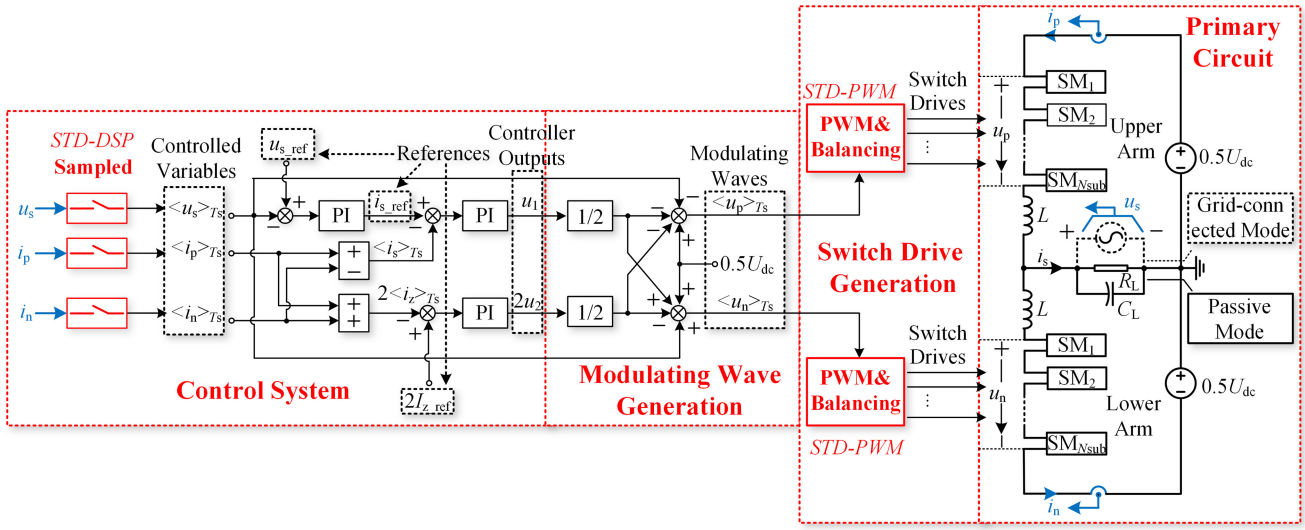

Fig. 4. Control strategy of the MMC system.

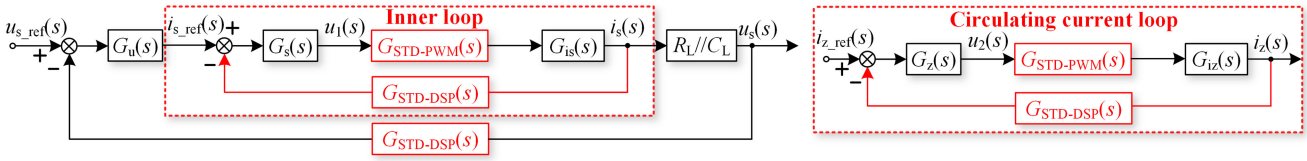

Fig. 5. Linear model of the MMC system considering the effects of the STD-AC.

loop i_{s_ref}, u_{s_ref} and I_{z_ref}, respectively, can be obtained as

$$\text{Passive mode}: \begin{cases} u_{s\_ref} = \dfrac{MU_{dc}}{2}\sin(\omega_0 t) \\ 2I_{z\_ref} = \dfrac{\max(\langle u_s \rangle_{T_s} \cdot \langle i_s \rangle_{T_s} \cos\varphi)}{U_{dc}} \end{cases}$$

Grid-connected mode :

$$\begin{cases} i_{s\_ref} = \sqrt{2}\dfrac{\sqrt{P^2+Q^2}}{U_s}\sin\left(\omega_0 t + \arctan\dfrac{Q}{P}\right) \\ 2I_{z\_ref} = \dfrac{2P}{U_{dc}} \end{cases} \tag{9}$$

where $\cos\varphi$ is the power factor, M is the modulation ratio, P and Q are the active and reactive power of the system, respectively. The outer loop is not present when the MMC operates as a grid-connected inverter, and i_{s_ref} is directly determined by (9). Conversely, the references i_{s_ref} of the inner loop is determined by the outer loop controller when the MMC operates as a passive inverter. In addition, the sampled and PWM processes, which are marked in red boxes, are introduced into the system, and the corresponding STD are considered as well. The sampling gains of the voltages and currents are both set to one to simplify the analysis.

Furthermore, by using a Laplace transformation in the small signal equations of (6), the transfer function $G_{is}(s)$ from $u_1(s)$ to $i_s(s)$ and $G_{iz}(s)$ from $u_2(s)$ to $i_z(s)$ can be obtained as

$$\begin{cases} G_{is}(s) = \dfrac{i_s(s)}{u_1(s)} = \dfrac{1}{sL} \\ G_{iz}(s) = \dfrac{i_z(s)}{u_2(s)} = \dfrac{1}{sL} \end{cases}. \tag{10}$$

The outer loop controller $G_u(s)$, the inner loop controller $G_s(s)$ and the circulating current controller $G_z(s)$ are described as

$$\begin{cases} G_u(s) = K_{P\_u} + K_{I\_u}/s \\ G_s(s) = K_{P\_is} + K_{I\_is}/s \\ G_z(s) = K_{P\_iz} + K_{I\_iz}/s \end{cases}. \tag{11}$$

The STD-DSP and STD-PWM are both present in the MMC system and should be considered in the linear model, whose transfer function can be described as

$$\begin{cases} G_{STD\text{-}DSP}(s) = \exp(-T_{STD\text{-}DSP}s) \\ G_{STD\text{-}PWM}(s) = \exp(-T_{STD\text{-}PWM}s) \end{cases}. \tag{12}$$

Therefore, the linear model considering the effects of the STD-AC in the system is shown in Fig. 5.

Based on Fig. 5, the open-loop transfer functions of the inner loop $G_{in}(s)$, circulating current loop $G_{izn}(s)$ and outer loop $G_{out}(s)$ can be described as (13) when the controller parameters

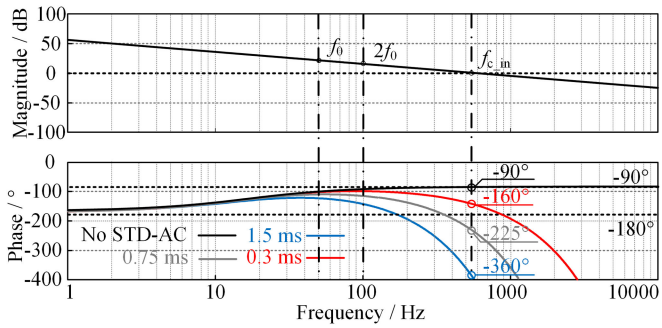

Fig. 6. Bode diagram of $G_{\text{in}}(s)$ with variations in f_s and $T_{\text{STD-AC}}$.

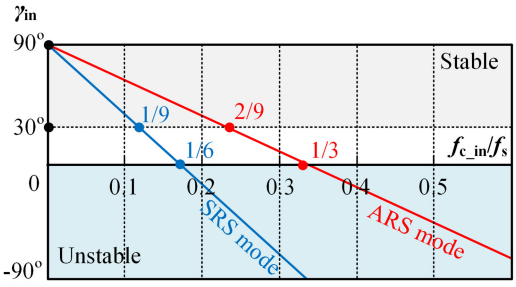

Fig. 7. Degree to which γ_{in} decreases in $G_{\text{in}}(s)$ with variations in f_{c_in}.

of $G_s(s)$ and $G_z(s)$ are the same.

$$\begin{cases} G_{\text{in}}(s) = G_{\text{izn}}(s) = G_s(s)G_{\text{STD-PWM}}(s)G_{is}(s) \\ \quad \times G_{\text{STD-DSP}}(s) = (K_{P\_\text{is}} + \dfrac{K_{I\_\text{is}}}{s})\dfrac{e^{-T_{\text{STD-AC}}s}}{sL} \\ G_{\text{out}}(s) = \dfrac{(K_{P\_\text{is}}s + K_{I\_\text{is}})(K_{P\_u}s + K_{I\_u})}{Ls^3 + s(K_{P\_\text{is}}s + K_{I\_\text{is}})e^{-T_{\text{STD-AC}}s}} \\ \quad \times \dfrac{R_L e^{-T_{\text{STD-AC}}s}}{1 + R_L C_L s} \end{cases}. \quad (13)$$

Significantly, $G_{\text{out}}(s)$ is not present in the grid-connected mode but is present in the passive mode.

B. Effect of the STD-AC on the System Stability

Based on (13), $G_{\text{in}}(s)$ and $G_{\text{izn}}(s)$ have the same expression. Therefore, the system characteristics of the inner loop and circulating current loop can be studied at the same time. To quantitatively analyse the characteristics, a Bode diagram of $G_{\text{in}}(s)$ is required, as are the corresponding parameters $T_{\text{STD-AC}}$, L, K_{P_iz}, and K_{I_iz} in $G_{\text{in}}(s)$. Subsequently, $T_{\text{STD-AC}}$ are assumed to be 1.5, 0.75, and 0.3 ms, respectively, and the corresponding f_s values are 1, 2, and 5 kHz (η is set to 1 based on Table I), respectively, when the overall system operates in the SRS mode. Additionally, L is set to 3.6 mH.

Furthermore, the system characteristics primarily contain three components. The first is the transient response when a load, voltage, or current changes, necessitating that the cutoff frequency f_{c_in} of $G_{\text{in}}(s)$ have an adequate value. The second is the steady-state performance, including the steady-state error of the alternating current and the suppression ability of the circulating current, necessitating a sufficient magnitude of the magnitude–frequency characteristics of $G_{\text{in}}(s)$. The third is the system stability, necessitating a sufficient phase in the phase–frequency characteristics of $G_{\text{in}}(s)$, because the system will be unstable if the phase is smaller than $-180°$ at f_{c_in}. Therefore, the corresponding f_{c_in}, K_{p_is}, and K_{i_is} are set to 500 Hz, 11, and 1100, respectively. The corresponding Bode diagram of $G_{\text{in}}(s)$, which includes the magnitude–frequency and phase–frequency characteristics for different $T_{\text{STD-AC}}$ values, is shown in Fig. 6.

In Fig. 6, f_{c_in} remains at 500 Hz with variations in f_s. The phase is approximately $-90°$ at 500 Hz when the STD-AC is not present in the system, indicating that the system is stable. However, the phase has a significant decrease and reaches $-160°$ at f_{c_in} when $T_{\text{STD-AC}}$ is 0.3 ms. Furthermore, the phase is smaller than $-180°$ when $T_{\text{STD-AC}}$ is 1.5 ms and 0.75 ms, indicating that the system is unstable. Therefore, the phase of $G_{\text{in}}(s)$ at f_{c_in} decreases rapidly with decreases in f_s and increases in $T_{\text{STD-AC}}$. The MMC system is even unstable when f_s decreases to a low value and the corresponding $T_{\text{STD-AC}}$ reaches to a great value. Consequently, the STD-AC has a significant effect on the system stability, and cannot be neglected in MMC systems.

C. Effect of the STD-AC on the Transient Response and Steady-State Performance

Furthermore, to provide a more intuitive description of the decrease in stability, the phase margin γ_{in} of $G_{\text{in}}(s)$ can be approximated as (14) based on (13) when η is set to 1

$$\begin{aligned} \gamma_{\text{in}} &\approx 90° - 360° T_{\text{STD-AC}} f_{c\_\text{in}} \\ &= \begin{cases} 90°\left(1 - 6 \cdot \dfrac{f_{c\_\text{in}}}{f_s}\right) < 90°, & \text{in the SRS mode} \\ 90°\left(1 - 3 \cdot \dfrac{f_{c\_\text{in}}}{f_s}\right) < 90°, & \text{in the ARS mode} \end{cases}. \end{aligned} \quad (14)$$

In (14), γ_{in} is always smaller than 90°, indicating that the STD-AC inevitably decreases the system stability regardless of the $T_{\text{STD-AC}}$ value. A group of curves based on (14) is used to describe the degree to which γ_{in} decreases with increases in the ratio of f_{c_in} and f_s, $G_{\text{in}}(s)$ in Fig. 7.

In Fig. 7, γ_{in} decreases rapidly with increases in f_{c_in}/f_s. γ_{in} can be greater than 30° and satisfy the smallest phase margin that the system stability requires when f_{c_in}/f_s is smaller than 1/9 in the SRS mode and smaller than 2/9 in the ARS mode. Conversely, γ_{in} is smaller than zero when f_{c_in}/f_s is greater than 1/6 in the SRS mode and greater than 1/3 in the ARS mode, making the system unstable. Therefore, γ_{in} and f_{c_in}/f_s are negatively correlated, and f_{c_in} should be decreased to a proper value of f_s such that γ_{in} reaches a value at which the system can be stable. Consequently, the system transient response is slower with decreases in f_{c_in} under the effect of the STD-AC.

Subsequently, to describe the steady-state performance of the system with decreases in f_{c_in}, a new Bode diagram is shown in Fig. 8 for f_{c_in} decreasing from 500 to 200 and 100 Hz, and the corresponding γ_{in} simultaneously increases from $-45°$ to 33°

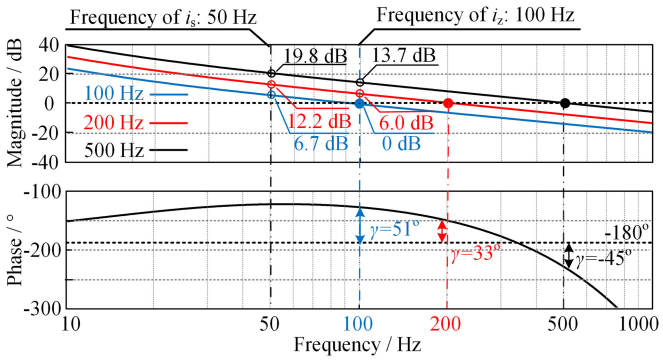

Fig. 8. Bode diagram of $G_{\rm in}(s)$ with variations in the cutoff frequency $f_{c-{\rm in}}$.

and 51°, respectively. In addition, $T_{\text{STD-AC}}$ is set to 0.75 ms, and the corresponding f_s is 2 kHz.

In Fig. 8, the phase-frequency characteristics of $G_{\rm in}(s)$ remain the same while the magnitude-frequency characteristics are varied. $f_{c\_{\rm in}}$ initially decreases from 500 to 200 Hz and the corresponding $\gamma_{\rm in}$ increases from $-45°$ to 33°, satisfying the demands of the system stability. However, the magnitudes of $G_{\rm in}(s)$ at f_0 and $2f_0$ decrease from 13.7 to 6.0 dB and from 19.8 to 12.2 dB, respectively. The magnitudes of $G_{\rm in}(s)$ at f_0 and $2f_0$ have greater decreases when $f_{c\_{\rm in}}$ decreases to 100 Hz.

Furthermore, the difference between the alternating current i_s and its reference $i_{s\_{\rm ref}}$ can be defined as the steady-state error $e_{is}(\omega_0 t)$, and the difference between the circulating current i_z and its reference $I_{z\_{\rm ref}}$ can be defined as the steady-state error $e_{iz}(2\omega_0 t)$. $e_{\rm is}(\omega_0 t)$ and $e_{iz}(2\omega_0 t)$ can be described as (15) based on Fig. 5:

$$\begin{cases} e_{is}(\omega_0 t) = i_{s\_\rm ref} - i_s \\ = \left|\dfrac{1}{1+G_{\rm in}(s)}\right|_{s=j\omega_0} \times i_{s\_\rm ref}\left(\omega_0 t - \left|\dfrac{1}{1+G_{\rm in}(s)}\right|_{s=j\omega_0}\right) \\ \approx \dfrac{1}{|G_{\rm in}(s)|_{s=j\omega_0}} i_{s\_\rm ref}\left(\omega_0 t - \left|\dfrac{1}{G_{\rm in}(s)}\right|_{s=j\omega_0}\right) \\ e_{iz}(2\omega_0 t) = I_{z\_\rm ref} - i_z \\ = -\left|\dfrac{1}{1+G_{\rm in}(s)}\right|_{s=j2\omega_0} \times i_{z0}\left(2\omega_0 t - \left|\dfrac{1}{1+G_{\rm in}(s)}\right|_{s=j2\omega_0}\right) \\ \approx \dfrac{-1}{|G_{\rm in}(s)|_{s=j2\omega_0}} i_{z0}\left(2\omega_0 t - \left|\dfrac{1}{G_{\rm in}(s)}\right|_{s=j2\omega_0}\right) \end{cases} \tag{15}$$

where $i_{z0}(2\omega_0 t)$ is the alternating component of initial circulating current. Based on (15), the amplitudes of $e_{is}(\omega_0 t)$ and $e_{iz}(2\omega_0 t)$ are inversely proportional to the magnitudes of $G_{\rm in}(s)$ at f_0 and $2f_0$, respectively. Thus, decreases in the magnitudes in $G_{\rm in}(s)$ can directly lead to increases in the steady-state errors of the alternating current and circulating current. Because suppression of the circulating current is to limit i_z to $I_{z\_\rm ref}$, the increase of $e_{iz}(2\omega_0 t)$ demonstrates that the ability to suppress the circulating current is simultaneously weaken.

The above analysis demonstrates that STD-AC can lead to a significant phase decrease in the inner loop and circulating current loop, which greatly reduces the system stability. Thus, the effects of the STD-AC should be rigorously considered in the design of the MMC system controller parameters. Furthermore, to ensure the system stability under the STD-AC effects, the cutoff frequency $f_{c\_{\rm in}}$ cannot be set to an applicable value, and thus cannot satisfy the demands of the system transient response and steady-state performance.

IV. Optimal Design Method Under the STD-AC Effects

Based on the analysis above, the STD-AC decreases the stability, steady-state performance and transient response of the MMC system. Therefore, this paper proposes an optimal design method of the sampling frequency $f_{\rm sa}$ and controller parameters to decrease the effects of the STD-AC. Because $T_{\text{STD-AC}}$ has different values in the overall system and distributed system based on Table I, the optimal design method includes two components, as detailed below.

A. Optimal Design Method in the Overall System

The cutoff frequency $f_{c\_{\rm in}}$ is the most significant parameter of the system because it is closely related to the stability, steady-state performance and transient response of the system based on the analysis in Section III. Therefore, $f_{c\_{\rm in}}$ should be determined first.

Theoretically, the alternating voltage u_s and alternating current i_s can be transformed from ac variables into dc variables in a three-phase MMC system. Because the dc variables have a lower rate of change compared to the ac variables, the system with a PI controller has a good steady-state performance and transient response of the dc variables even if $f_{c\_{\rm in}}$ is set to a low value. However, many ac harmonics are present in the alternating voltage and current, thus decreasing the effect of the dc controlling method. In addition, the three-phase unbalanced phenomenon can also reduce the control effect. Therefore, a method that controls the ac variables directly has been widely used. However, this method requires a higher $f_{c\_{\rm in}}$ of the system to follow the change rate of the ac variables.

$f_{c\_{\rm in}}$ is typically set to 1/10 the value of f_s in a two-level converter to avoid the STD effects. However, f_s can decrease to 500 Hz or lower in the MMC system, and $f_{c\_{\rm in}}$ can correspondingly decrease to 100 Hz or lower when $f_{c\_{\rm in}}$ is still set to 1/10 the value of f_s. Such a low $f_{c\_{\rm in}}$ cannot satisfy the system steady-state performance and transient response. Zhao [35] considered that $f_{c\_{\rm in}}$ could set to $N_{\rm sub}/10$ the value of f_s. However, this method makes $f_{c\_{\rm in}}$ linearly related to $N_{\rm sub}$ and causes $f_{c\_{\rm in}}$ to be overly high or low when $N_{\rm sub}$ changes, which is also not applicable. This paper considers that $f_{c\_{\rm in}}$ should be related to the fundamental frequency of the controlled objects, such as i_s and i_z, rather than to f_s and $N_{\rm sub}$. Furthermore, a proper value of $f_{c\_{\rm in}}$ should satisfy three demands. The first is to satisfy the speed of the transient response, requiring that $f_{c\_{\rm in}}$ be at least ten times greater than the fundamental frequency f_0 of i_s. The second is that the amplitude of the steady error $e_{is}(\omega_0 t)$ should be smaller than 5% of the reference $i_{s\_\rm ref}$, requiring that $f_{c\_{\rm in}}$

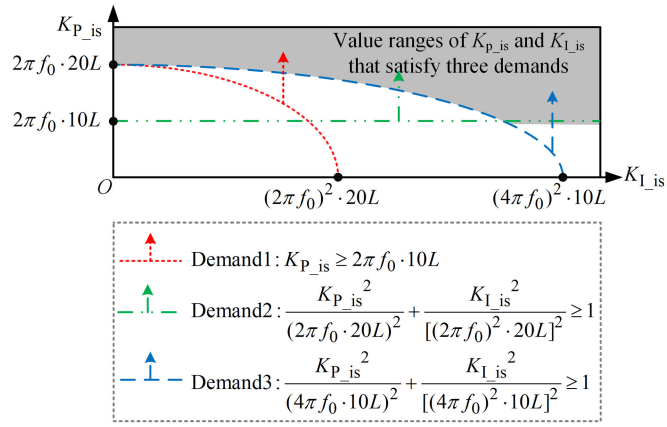

Fig. 9. Value ranges of K_{P_is} and K_{I_is} under three demands.

is set such that the magnitude of $G_{\text{in}}(s)$ at f_0 is greater than 20 based on (15). The third is to suppress the circulating current i_z and make the amplitude of $e_{iz}(2\omega_0 t)$ smaller than 10% of I_{z_ref}, requiring that f_{c_in} is set such that the magnitude of $G_{\text{in}}(s)$ at $2f_0$ is greater than 10 based on (15). These demands can be quantitatively described as

$$\begin{cases} f_{c\_\text{in}} = \dfrac{1}{2\pi}\sqrt{\dfrac{K_{P\_is}^2 + \sqrt{(-K_{P\_is}^2)^2 + 4L^2 K_{I\_is}^2}}{2L^2}} \\ \approx \dfrac{K_{P\_is}}{2\pi L} \geq 10 f_0 \qquad \text{Demand 1} \\ |G_{\text{in}}(s)|_{s=j\omega_0} = \dfrac{K_{I\_is}}{(2\pi f_0)^2 L}\sqrt{\dfrac{K_{P\_is}^2}{K_{I\_is}^2}(2\pi f_0)^2 + 1} \\ \geq 20 \qquad \text{Demand 2} \\ |G_{\text{in}}(s)|_{s=j2\omega_0} = \dfrac{K_{I\_is}}{(2\cdot 2\pi f_0)^2 L}\sqrt{\dfrac{K_{P\_is}^2}{K_{I\_is}^2}(2\cdot 2\pi f_0)^2 + 1} \\ \geq 10 \qquad \text{Demand 3} \end{cases} \tag{16}$$

Based on (16), K_{P_is} and K_{I_is} have value ranges rather than being equal to specific values. Therefore, the functional image shown in Fig. 9 is used to describe the value ranges of K_{P_is} and K_{I_is} under the three demands.

In Fig. 9, K_{I_is} can be set to any value that is greater than zero to satisfy the system demands when K_{p_is} is greater than $40\pi L f_0$. Therefore, to simplify the selection of the controller parameters, the values of $f_{c\_\text{in}}, K_{P\_is}, K_{I\_is}, K_{P\_iz}$, and K_{I_iz} can be obtained as

$$\begin{cases} f_{c\_\text{in}} \geq 20 f_0, K_{P\_is} = K_{P\_iz} \approx 2\pi L f_{c\_\text{in}} \geq 40\pi L f_0 \\ K_{I\_is} = K_{I\_iz} = \begin{cases} 100 K_{P\_is} & \text{in a continuous system} \\ 100 K_{P\_is}/f_{\text{sa}} & \text{in a discrete system} \end{cases} \end{cases} . \tag{17}$$

The minimum of γ_{in} should also be greater than 30°, which can be described in (18) based on (14) and Table I.

$$\begin{aligned} \gamma_{\text{in}} &\approx 90^\circ - 360^\circ T_{\text{STD-AC}} f_{c\_\text{in}} \\ &= 90^\circ - 360^\circ (0.5+\eta) T_{\text{sa}} f_{c\_\text{in}} \geq 30^\circ. \end{aligned} \tag{18}$$

TABLE II
RECOMMENDED MINIMUM VALUES OF f_{sa} FOR DIFFERENT f_s

f_s (kHz)	0.25	0.5	1	2	3	4	5
f_{sa} (kHz, $\eta = 0.2$)	4.5	4.5	5	6	6	8	5
f_{sa} (kHz, $\eta = 1$)	9.5	9.5	10	10	12	12	10

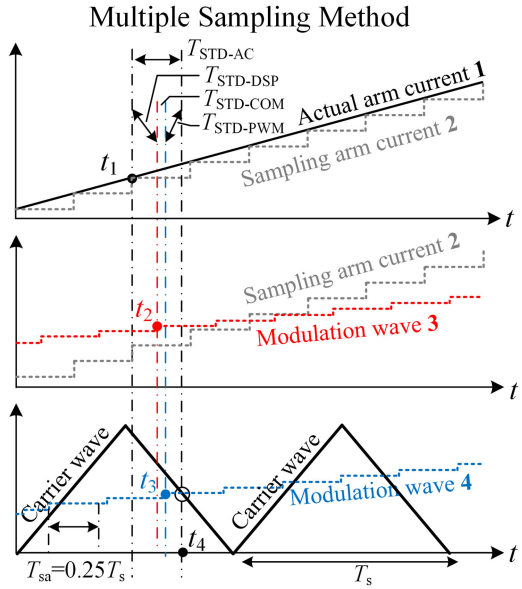

Fig. 10. Quantitative relations between $T_s, T_{\text{sa}}, T_{\text{STD-DSP}}, T_{\text{STD-COM}}$, and $T_{\text{STD-PWM}}$ in the multiple-sampling method.

Therefore, the minimum of the sampling frequency f_{sa} can be solved as

$$f_{\text{sa}} = \frac{1}{T_{\text{sa}}} \geq (3+6\eta) f_{c\_\text{in}}. \tag{19}$$

The η can be set to 1 to satisfy the worst possible case. However, using an asynchronous bus to transfer the modulation waves and optimizing the control algorithm in an overall system allows η to be approximately 0.2 or smaller. Furthermore, the value of f_{sa} is best set to an integer times the value of f_s to avoid voltage and current distortions. Therefore, the recommended minimum values of f_{sa} when f_0 and f_{c_in} are equal to 50 Hz and 1 kHz, respectively, are shown in Table II.

Because f_{sa} is greater than f_s in Table II, a multiple-sampling method [34] that was used in dc–dc converters is introduced into the MMC system to directly increase f_{sa} and decrease $T_{\text{STD-AC}}$, as shown in Fig. 10.

B. Optimal Design Method in the Distributed System

$T_{\text{STD-COM}}$ is substantial in a distributed system, thus making $T_{\text{STD-AC}}$ increase and limiting the value of f_{c_in}, which can be described as (20) based on (18)

$$f_{c\_\text{in}} < \frac{1}{(3+6\eta)T_{\text{sa}} + 6T_{\text{STD-COM}}} < \frac{1}{6T_{\text{STD-COM}}}. \tag{20}$$

Based on (20) and Table I, f_{c_in} should be set to a value that is always smaller than $1/6T_{\text{STD-COM}}$ regardless of the value of f_{sa}. Furthermore, (20) can be defined as the fourth demand of

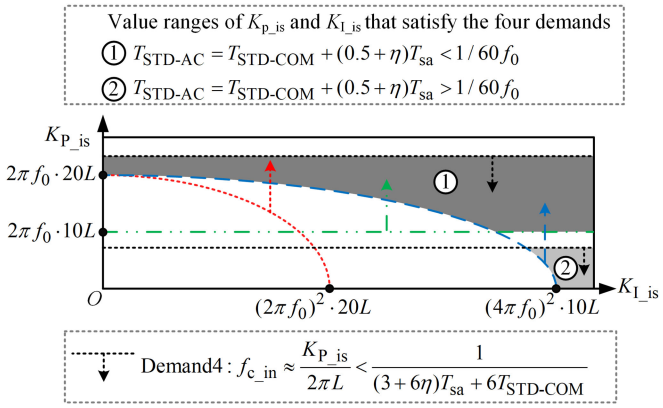

Fig. 11. Value ranges of K_{P_is} and K_{I_is} under the four demands.

f_{c_in} in a distributed MMC system. The value ranges of K_{P_is} and K_{I_is} under the four demands are shown in Fig. 11.

In Fig. 11, K_{P_is} and K_{I_is} can have the applicable values in cycle 1 to satisfy the four demands when $T_{STD\text{-}AC}$ is smaller than $1/60f_0$. However, K_{P_is} and K_{I_is} cannot satisfy the first demand that f_{c_in} should be greater than $10f_0$ when $T_{STD\text{-}COM}$ is greater than $1/60f_0$, and thus cannot have the applicable values in cycle 1. Therefore, the first demand have to be eliminated even if the speed of the system transient response is decreased, and consequently K_{P_is} and K_{I_is} can have the applicable values in cycle 2.

C. Optimal Design Method in the Outer Loop

In certain applications, the MMC operates in a passive mode, and the alternating voltage must be controlled. Therefore, K_{p_u} and K_{i_u} in the outer loop transfer function $G_{\text{outer}}(s)$ must be designed and can be approximated by

$$G_{\text{out}}(s) \approx \frac{K_{I\_u}R}{1+R_LC_Ls} \frac{(\frac{K_{P\_u}}{K_{I\_u}}s+1)}{s(\frac{Ls}{K_{P\_is}}e^{\text{STD-AC}s}+1)} \approx \begin{cases} \frac{K_{I\_u}}{C_Ls^2}\left(\frac{K_{P\_u}}{K_{I\_u}}s+1\right) & \text{in an empty load} \\ \frac{K_{I\_u}R_L}{s}\left(\frac{K_{P\_u}}{K_{I\_u}}s+1\right) & \text{in a full load} \end{cases} \tag{21}$$

where f_{c_out} is the cutoff frequency of $G_{\text{outer}}(s)$, which reaches its highest point under an empty load and decreases to its minimum value under a full load. R_L is the equivalent load resistor. However, a proper value of f_{c_out} should still satisfy all three demands. The first is to satisfy the speed of the transient response in $G_{\text{outer}}(s)$ when the load changes. However, f_{c_out} should be slower than the speed of $G_{\text{in}}(s)$, requiring that f_{c_out} be smaller than ten times the value of f_0 in the empty-load mode but greater than five times the value of f_0 in the full-load mode. The second is to decrease the steady-state error of u_s, which requires that the magnitude of $G_{\text{out}}(s)$ at f_0 be greater than ten in the full-load mode. The third is to ensure the stability of $G_{\text{outer}}(s)$.

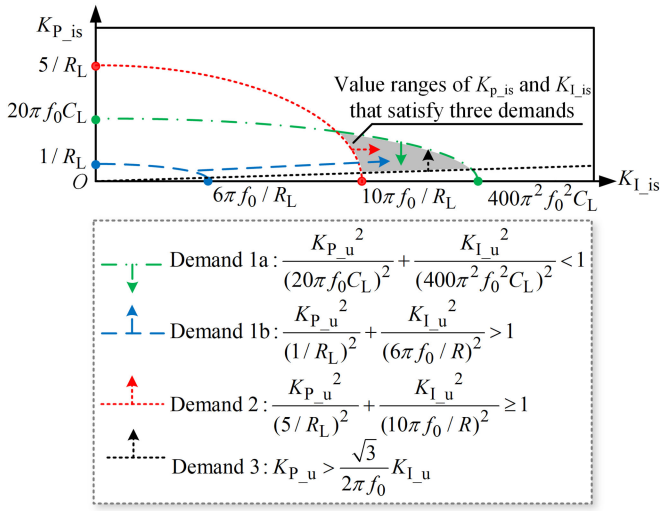

Fig. 12. Value ranges of K_{P_is} and K_{I_is} under the three demands.

These demands can be quantitatively described as

$$\begin{cases} |G_{\text{out}}(s)|_{s=j10\omega_0} = \frac{1}{(10\cdot 2\pi f_0)^2 C_L} \cdot \\ \sqrt{(K_{P\_u}10\cdot 2\pi f_0)^2 + K_{I\_u}{}^2} < 1 \qquad \text{Demand 1a} \\ |G_{\text{out}}(s)|_{s=j5\omega_0} = \frac{R_L}{3\omega_0}\sqrt{(K_{P\_u}3\cdot 2\pi f_0)^2 + K_{I\_u}{}^2} \\ > 1 \qquad \text{Demand 1b} \\ |G_{\text{out}}(s)|_{s=j\omega_0} = \frac{R_L}{\omega_0}\sqrt{(K_{P\_u}\cdot 2\pi f_0)^2 + K_{I\_u}{}^2} \\ \geq 10 \qquad \text{Demand 2} \\ 180^\circ + \arg|G_{\text{out}}(s)|_{s=j10\omega_0} \approx 180^\circ + \\ \arctan\frac{K_{P\_u}10\cdot 2\pi f_0}{K_{I\_u}} > 30^\circ \qquad \text{Demand 3} \end{cases} . \tag{22}$$

Based on (22), the functional image that is shown in Fig. 12 is used to describe the value ranges of K_{P_is} and K_{I_is}.

In Fig. 12, K_{P_is} and K_{I_is} can attain the applicable values to satisfy three demands. The design methods above allow the system to simultaneously satisfy the demands of the transient response, steady-state performance and stability under the effects of the STD-AC.

V. Experimental Results

The experiments in this study are performed using a single-phase MMC platform with eight submodules, as shown in Fig. 13.

The experimental platform operates in a passive mode to avoid the impact of distortion in the power grid. The control strategy, capacitor voltage balancing strategy, and switch generation method are implemented in the main control system with DSP (TMS320F28335) and FPGA (EP3C5E144I7). Dedicated switch-drive lines and CAN-bus communication lines are used

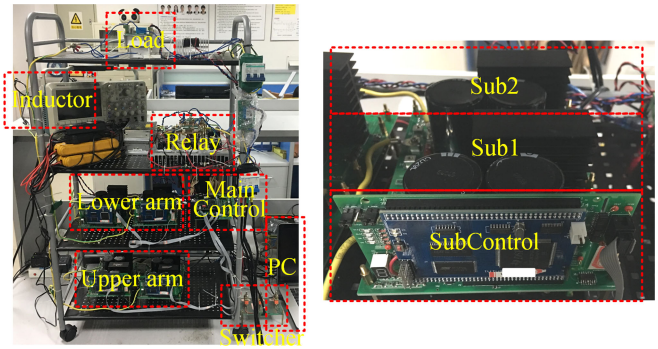

Fig. 13. Experimental platform of the MMC system.

TABLE III
PARAMETERS USED IN THE MMC SYSTEM

Parameter	Symbol	Value	Parameter	Symbol	Value
Direct Voltage (Input)	$U_{\rm dc}$	400 V	STD-PWM	$T_{\text{STD-PWM}}$	80 μs
Alternating Voltage (Output, RMS)	U_s	110 V	STD-AC	$T_{\rm STD-AC}$	0.11 ms
Alternating Current (Output, RMS)	I_s	18.2 A	Proportional Gain in $G_{\rm out}(s)$	K_{P_u}	0.3
Active Power	P	2 kW	Integral Gain in $G_{\rm out}(s)$	K_{1_u}	800/2000
Arm Inductor	L	3.6 mH	Proportional Gain in $G_{\rm in}(s)$	$K_{P\_is}(K_{P\_iz})$	23
Submodule Capacitor	C	2200 μF	Integral Gain in $G_{\rm in}(s)$	$K_{1\_is}(K_{1\_iz})$	2300/2000
Switching Frequency	f_s	2 kHz	Cut-off Frequency in $G_{\rm out}(s)$	$f_{c\_\rm out}$	300 Hz
Sampling Frequency	$f_{\rm sa}$	6 kHz	Phase Margin in $G_{\rm out}(s)$	$\gamma_{\rm out}$	87°
STD-DSP	$T_{\rm STD-DSP}$	30 μs	Cut-off Frequency in $G_{\rm in}(s)$	$f_{c\_\rm in}$	1 kHz
STD-COM	$T_{\rm STD-COM}$	Neglected	Phase Margin in $G_{\rm in}(s)$	$\gamma_{\rm in}$	50°

between the main control system and submodules, where a DSP (TMS320F2812) is used in the subcontrol system. The parameters that were used in the MMC system are listed in Table III.

The amplitudes of the alternating voltage, arm current, and circulating current in the control system are the same as in the primary circuit when using an equal-amplitude sampling algorithm in the DSP.

A. Comparison of the Alternating Voltage, Current, and Circulating Current With Different Switching Frequencies

In this section, the system operates in the SRS mode, where f_s is equal to $f_{\rm sa}$. The f_s are set to 1, 2, and 5 kHz to change the value of $T_{\text{STD-AC}}$. However, based on Fig. 6 and (14), the system cannot be stable when f_s is set to 1 kHz and 2 kHz and the $f_{c\_\rm in}$ are set to 500 Hz. Significantly, the system cannot operate in an unstable state because it can cause an overvoltage and overcurrent that can damage the system. Therefore, the $f_{c\_\rm in}$ decrease and the corresponding controller parameters are changed to stabilize the system. In addition, the outer loop is eliminated to avoid affecting the stability of the inner loop and circulating current loop. The changed parameters in this section are shown in Table IV.

TABLE IV
CHANGED PARAMETERS OF THE MMC SYSTEM

Symbol	Fig. 14(a)	Fig. 14(b)	Fig. 14(c)	Fig. 16(a)	Fig. 16(b)
f_s (kHz)	1	2	5	2	2
$f_{\rm sa}$ (kHz)	1	2	5	2	2
$T_{\rm STD-DSP}$ (ms)	1	0.5	0.2	0.5	0.5
$T_{\rm STD-PWM}$ (ms)	0.5	0.25	0.1	0.25	0.25
$T_{\rm STD-AC}$ (ms)	1.5	0.75	0.3	0.75	0.75
$K_{P\_is}(K_{P\_iz})$	3.4	7.1	11	4.5	2.2
$K_{1\_is}(K_{1\_iz})$	340/1000	710/2000	1100/5000	450/2000	220/2000
$f_{c\_\rm in}$ (Hz)	150	313	500	200	100
$\gamma_{\rm in}$(deg)	5	5	37	33	51

TABLE V
THDS OF THE ALTERNATING VOLTAGE AND CURRENT IN FIG. 14

f_s (kHz)	1	2	5
THDs in u_s	13.0%	6.9%	0.3%
THDs in i_s	20.6%	13.9%	0.9%

Fig. 14 shows the waveforms of the alternating voltage u_s, alternating current i_s, and circulating current i_z with different switching frequencies f_s. In Fig. 14(a), f_s is set to 1 kHz and $T_{\text{STD-AC}}$ is 1.5 ms, causing u_s and i_s to be highly distorted because of the low phase margin (5°). Large steady-state errors occur in i_s because of the low $f_{c\_\rm in}$ and low magnitude of $G_{\rm in}(s)$. Furthermore, i_z fluctuates considerably and is completely uncontrolled. In Fig. 14(b), f_s is set to 2 kHz and $T_{\text{STD-AC}}$ equals 0.75 ms, causing u_s and i_s to be highly distorted with i_z also uncontrolled. In Fig. 14(c), f_s is set to 5 kHz and $T_{\text{STD-AC}}$ equals 0.3 ms, which does not cause u_s and i_s to be distorted. Subsequently, i_z fluctuates only slightly, with a dc bias of 5 A, indicating that the circulating current is adequately suppressed. However, the system has a higher frequency than that of the original system design, and the switching losses increase accordingly.

Furthermore, the total harmonic distortions (THDs) of u_s and i_s in Fig. 14(a)–(c) are listed in Table V, and the corresponding spectrums are shown in Fig. 15(a) and (b), respectively. Significantly, the MMC system with lower switching frequency and higher $T_{\text{STD-AC}}$ has higher proportion of low frequency harmonics and higher THD in the alternating voltage and current, consequently is closer to an unstable state.

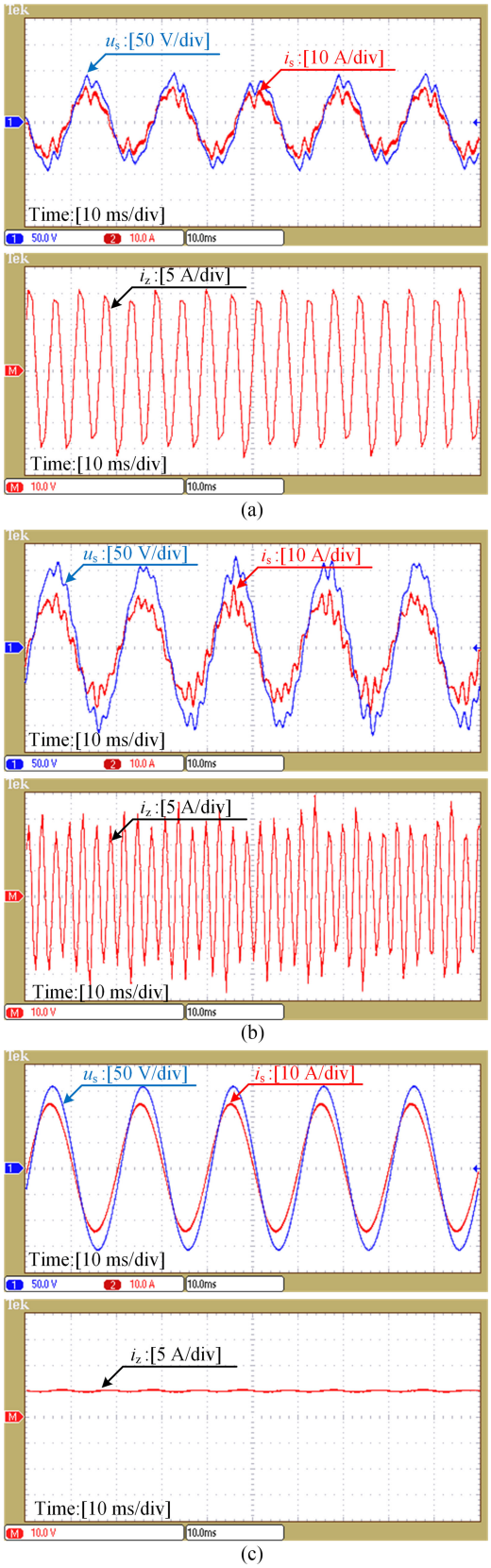

Fig. 14. Waveforms of the alternating voltage u_s, alternating current i_s and circulating current i_z with different switching frequencies f_s: a) 1 kHz, b) 2 kHz, and c) 5 kHz.

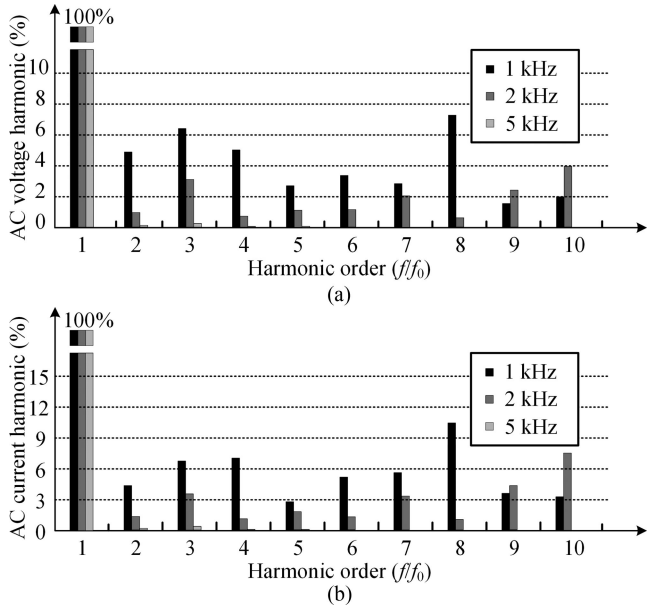

Fig. 15. Spectrums of the alternating voltage u_s and current i_s with different switching frequencies f_s: (a) u_s and (b) i_s.

The experimental results verify the conclusions presented above: The STD-AC can cause a considerable decrease in the phase margin, making the MMC system unstable and distorting the voltages and currents when f_s decreases to a low value and the corresponding $T_{\text{STD-AC}}$ reaches a high value.

B. Comparison of the Alternating Voltage, Currents, and Circulating Current With Different Cutoff Frequencies

In this section, the system operates at the switching frequency f_s of 2 kHz, and the corresponding $T_{\text{STD-AC}}$ is 0.75 ms. To make γ_{in} greater than 30° which is the minimum requirement of the phase margin for the system stability, the system decreases the cutoff frequency f_{c_in} from 313 Hz in Section A to 200 and 100 Hz. Therefore, the corresponding γ_{in} reaches 33° and 51°, thus satisfying the phase margin demand. Furthermore, the active power P changes from 1 to 2 kW to test the transient response during the system operating. In addition, the outer loop is eliminated to avoid affecting the inner loop and circulating current loop. The changed parameters in this section are shown in Table IV.

Fig. 16 and Table VI show the waveforms and corresponding measurement results of the alternating voltage u_s, alternating current i_s and circulating current i_z with different cutoff frequency f_{c_in}. In addition, amplitude error of i_s is defined as the amplitude ratio between the steady-state error $(i_{s\_\text{ref}} - i_s)$ and reference i_{s_ref}, and fluctuation range of i_z is defined as the amplitude ratio between the steady-state error $(I_{z\_\text{ref}} - i_z)$ and reference I_{z_ref}. In Fig. 16(a), f_{c_in} is set to 200 Hz, γ_{in} is 33°, and the corresponding THDs of u_s and i_s are far smaller than that in Fig. 14(b). Therefore, the alternating voltage and current are not distorted and the system is stable. However, great amplitude errors of i_s (14.9% at 1 kW and 4.6% at 2 kW in Table VII)

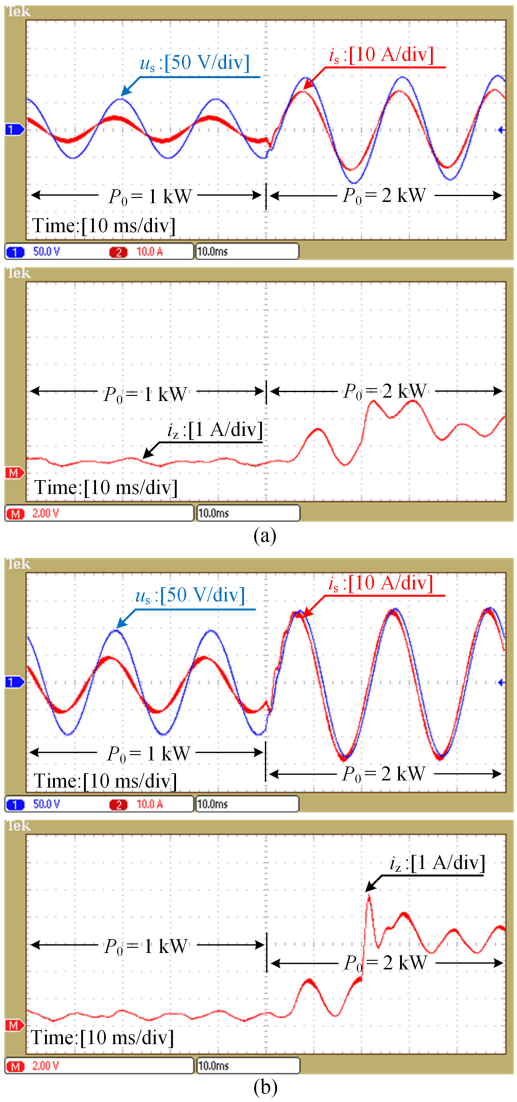

Fig. 16. Waveforms of the alternating voltage u_s, alternating current i_s, and circulating current i_z with different cutoff frequencies $f_{c-\text{in}}$: a) $f_{c-\text{in}}$ is equal to 200 Hz and b) $f_{c-\text{in}}$ is equal to 100 Hz.

TABLE VI
MEASUREMENT RESULTS OF THE ALTERNATING VOLTAGE, ALTERNATING CURRENT, AND CIRCULATING CURRENT IN FIG. 16

f_{c_in}, P	Stability		Steady-state Performance		Transient Response	
	THD of u_s (%)	THD of i_s (%)	Amplitude Error of i_s (%)	Fluctuation Range of i_z (%)	Regulation Time (ms)	Overshoot (%)
200 Hz, 1 kW	0.2	5.6	14.9	34.2	4	None
200 Hz, 2 kW	0.2	2.4	4.6	16.9		
100 Hz, 1 kW	0.4	12.5	51.3	83.3	6	3.3
100 Hz, 2 kW	0.3	3.0	38.2	38.5		

TABLE VII
MEASUREMENT RESULTS OF THE ALTERNATING VOLTAGE, ALTERNATING CURRENT, AND CIRCULATING CURRENT IN FIG. 17

f_{c_in}, P	Stability		Steady-State Performance		Transient Response	
	THD of u_s (%)	THD of i_s (%)	Amplitude Error of i_s (%)	Fluctuation Range of i_z (%)	Regulation Time (ms)	Overshoot (%)
1 kHz, 1 kW	0.2	4.9	2.3	8.4	2	None
1 kHz, 2 kW	0.2	2.4	0.7	4.9		

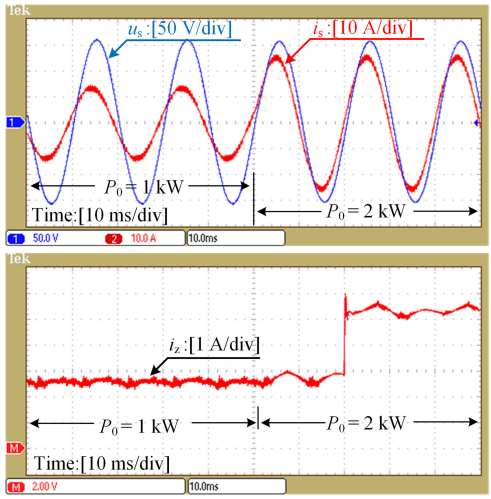

Fig. 17. Waveforms of the alternating voltage u_s, alternating current i_s, and circulating current i_z when cutoff frequencies $f_{c-\text{in}}$ equals 1 kHz and switching frequencies f_s equals 2 kHz.

occur because of a low f_{c_in} and corresponding low magnitude of $G_{\text{in(s)}}$. Furthermore, i_z fluctuates considerably at the same time (34.2% at 1 kW and 16.9% at 2 kW in Table VII). Consequently, the steady-state performance is poor when f_{c_in} is 200 Hz. In Fig. 16(b), f_s is set to 100 Hz, γ_{in} is 51°, and the system has a worse steady-state performance because steady-state errors of i_s and fluctuation range of i_z both increase based on Table VII. The regulation time and overshoot of i_s in Fig. 16(b) are greater than that in Fig. 16(a), indicating that the transient response is more poor when f_{c_in} decreases.

The experimental results verify the conclusions presented above: considering the effects of the STD-AC, the cutoff frequency f_{c_in} is forcibly decreased to make the phase margin γ_{in} satisfy the demands of system stability. However, a low f_{c_in} and corresponding low magnitude of $G_{\text{in}}(s)$ lead to significant steady-state errors in the alternating current, decrease the suppression ability of the circulating current and give the system a poor transient response when the load changes.

C. Effect of the Optimal Design Method

The parameters used in this section are the same as in Table II. Fig. 17 and Table VII show the waveforms and corresponding

measurement results of the alternating voltage u_s, alternating current i_s, and circulating current i_z when the controller parameters are optimally designed based on the method presented in Section IV.

In Fig. 17 and Table VII, the MMC system is stable because u_s and i_s have limited distortions with small THDs. Furthermore, the system has a perfect steady-state performance and high-speed transient response because the corresponding steady-state errors, fluctuation ranges, regulation time, and overshoot in Table VII are considerably smaller than that in Table VI before the optimal design.

These experimental results verify that the optimal design in the controller parameters can effectively mitigate the deteriorations caused by the STD and provide effectively optimization for the performance of MMC systems.

VI. Conclusion

Three conclusions can be drawn from the results of this study.

1) STD can lead to a large phase decrease in the inner loop of the MMC system, considerably reducing the system stability.
2) Considering the STD effects, the cutoff frequency is forcibly decreased to make the phase margin satisfy the demands of system stability. However, a low cutoff frequency can give the system a poor transient response and steady-state performance, lead to a large steady-state error in the alternating current and decrease the suppression ability of the circulating current.
3) The experimental results confirm the presence of the deteriorations caused by the STD and demonstrate that the proposed optimal design methods can effectively mitigate these deteriorations, thus effectively optimizing the performance of an MMC system.

References

[1] M. Saeedifard and R. Iravani, "Dynamic performance of a modular multilevel back-to-back HVDC system," *IEEE Trans. Power Deliv.*, vol. 25, no. 4, pp. 2903–2912, Oct. 2010.

[2] J. Qin and M. Saeedifard, "Predictive control of a modular multilevel converter for a back-to-back HVDC system," *IEEE Trans. Power Deliv.*, vol. 27, no. 3, pp. 1538–1547, Jul. 2012.

[3] S. Debnath and M. Saeedifard, "A new hybrid modular multilevel converter for grid connection of large wind turbines," *IEEE Trans. Sustain. Energy*, vol. 4, no. 4, pp. 1051–1064, Oct. 2013.

[4] L. Harnefors, A. Antonopoulos, S. Norrga, L. Angquist, and H. Nee, "Dynamic analysis of modular multilevel converters," *IEEE Trans. Ind. Electron.*, vol. 60, no. 7, pp. 2526–2537, Jul. 2013.

[5] E. Solas, G. Abad, J. Barrena, A. Carcar, and S. Aurtenetxea, "Modelling, simulation and control of modular multilevel converter," in *Proc. Int. Power Electron. Motion Control Conf.*, 2010, pp. T2-90–T2-96.

[6] S. Debnath, J. Qin, B. Bahrani, M. Saeedifard, and P. Barbosa, "Operation, control, and applications of the modular multilevel converter: A review," *IEEE Trans. Power Electron.*, vol. 30, no. 1, pp. 37–53, Jan. 2015.

[7] C. Wang, L. Xiao, X. Zheng, L. Lv, Z. Xu, and X. Jiang, "Analysis, measurement, and compensation of the system time delay in a three-phase voltage source rectifier," *IEEE Trans. Power Electron.*, vol. 31, no. 8, pp. 6031–6043, Aug. 2016.

[8] Y. Zhang, H. Ma, C. Yang, and L. Dong, "Joint scheduling analysis of time-delay impact on networked control system for multi-inverter parallel operation," in *Proc. 36th Annu. Conf. IEEE Ind. Electron. Soc.*, 2010, pp. 2162–2167.

[9] H. Deng, R. Oruganti, and D. Srinivasan, "PWM methods to handle time delay in digital control of a UPS inverter," *IEEE Trans. Power Electron.*, vol. 3, no. 1, pp. 1–6, Mar. 2005.

[10] H. Shan, Y. Zhang, Y. Kang, X. Kong, and H. Li, "Research on one-step-delay effect of digital control PWM inverter," in *Proc. 31th Int. Telecommun. Energy Conf.*, 2009, pp. 1–4.

[11] R. Li, B. Liu, S. Duan, J. Yin, and X. Jiang, "Analysis of delay effects in single-loop controlled grid-connected inverter with LCL filter," in *Proc. IEEE Appl. Power Electron. Conf.*, 2013, pp. 329–333.

[12] H. Deng, R. Oruganti, and D. Srinivasan, "Adaptive digital control for UPS inverter applications with compensation of time delay," in *Proc. IEEE Appl. Power Electron. Conf.*, 2004, pp. 450–455.

[13] S. Kwak and J. Park, "Predictive control method with future zero-sequence voltage to reduce switching losses in three-phase voltage source inverters," *IEEE Trans. Power Electron.*, vol. 30, no. 3, pp. 1558–1566, Mar. 2015.

[14] Y. Wang, Z. Chen, X. Wang, Y. Tian, Y. Tan, and C. Yang, "An estimator-based distributed voltage-predictive control strategy for ac islanded micro grids," *IEEE Trans. Power Electron.*, vol. 30, no. 7, pp. 3934–3951, Jul. 2015.

[15] A. Bouafia, J. P. Gaubert, and F. Krim, "Predictive direct power control of three-phase pulse width modulation (PWM) rectifier using space-vector modulation (SVM)," *IEEE Trans. Power Electron.*, vol. 25, no. 1, pp. 228–236, Jan. 2010.

[16] S. Kwak, "Predictive control method with future zero-sequence voltage to reduce switching losses in three-phase voltage source inverters," *IEEE Trans. Power Electron.*, vol. 30, no. 3, pp. 1558–1566, Feb. 2014.

[17] Z. Song, Y. Tian, W. Chen, Z. Zou, and Z. Chen, "Predictive duty cycle control of three-phase active-front-end rectifiers," *IEEE Trans. Power Electron.*, vol. 31, no. 1, pp. 680–710, Jan. 2016.

[18] M. Preindl and S. Bolognani, "Model predictive direct speed control with finite control set of PMSM drive systems," *IEEE Trans. Power Electron.*, vol. 28, no. 2, pp. 1007–1015, Feb. 2013.

[19] S. Jeong and S. Song, "Improvement of predictive current control performance using online parameter estimation in phase controlled rectifier," *IEEE Trans. Power Electron.*, vol. 22, no. 5, pp. 1820–1825, Sep. 2007.

[20] Y. Zhang, W. Xie, Z. Li, and Y. Zhang, "Model predictive direct power control of a PWM rectifier with duty cycle optimization," *IEEE Trans. Power Electron.*, vol. 28, no. 11, pp. 5343–5351, Nov. 2013.

[21] C. Zou, B. Liu, S. Duan, and R. Li, "Influence of delay on system stability and delay optimization of grid-connected inverters with LCL filter," *IEEE Trans. Power Electron.*, vol. 10, no. 3, pp. 1775–1784, Aug. 2014.

[22] P. S. B. Nascimento, H.E.P. de Souza, F. A. S. Neves, and L. R. Limongi, "FPGA implementation of the generalized delayed signal cancelation—Phase locked loop method for detecting harmonic sequence components in three-phase signals," *IEEE Trans. Ind. Electron.*, vol. 60, no. 2, pp. 645–658, Feb. 2013.

[23] P. Sun, C. Liu, J. S. Lai, C. L. Chen, and N. Kees, "Three-phase dual-buck inverter with unified pulse width modulation," *IEEE Trans. Power Electron.*, vol. 27, no. 3, pp. 1159–1167, Mar. 2012.

[24] G. K. Hung, C. C. Chang, and C. L. Chen, "Analysis and implementation of a delay-compensated deadbeat current controller for solar inverters," *IEE Proc. Circuits Dev. Syst.*, vol. 148, no. 5, pp. 279–286, Oct. 2001.

[25] J. F. Stumper, V. Hagenmeyer, S. Kuehl, and R. Kennel, "Deadbeat control for electrical drives: A robust and performant design based on differential flatness," *IEEE Trans. Power Electron.*, vol. 30, no. 8, pp. 4585–4596, Aug. 2015.

[26] L. Hang, S. Liu, G. Yan, B. Qu, and Z. Lu, "An improved deadbeat scheme with fuzzy controller for the grid-side three-phase PWM boost rectifier," *IEEE Trans. Power Electron.*, vol. 26, no. 4, pp. 1184–1191, Apr. 2011.

[27] J. Hu and Z. Q. Zhu, "Improved voltage-vector sequences on dead-beat predictive direct power control of reversible three-phase grid-connected voltage-source converters," *IEEE Trans. Power Electron.*, vol. 28, no. 1, pp. 254–267, Jan. 2013.

[28] Z. Bao, Z. Wang, and S. Zhang, "A predictive deadbeat control in shunt active power filter," in *Proc. Int. Conf. Wirel. Commun. Signal Process.*, 2011, pp. 1–4.

[29] H. Liang, J. Kang, G. Li, and M Zhou, "A deadbeat control method for VSC-HVDC under ac voltage unbalance," in *Proc. IEEE Power Energy Soc. Gen. Meeting*, 2011, pp. 1–7.

[30] X. Zhang, W. Zhang, J. Chen, and D. Xu, "Deadbeat control strategy of circulating currents in parallel connection system of three-phase PWM converter," *IEEE Trans. Energy Convers.*, vol. 29, no. 2, pp. 406–417, Jun. 2014.

[31] J. Shibata, K. Ohishi, I. Ando, and M. Ogawa, "Fine output voltage control for inverter system having nonlinear load and time-delay," in *Proc. IEEE Power Electron. Conf.*, 2010, pp. 1541–1546.
[32] J. Wang, J. Yan, L. Jiang, and J. Zou, "Delay-dependent stability of single-loop controlled grid-connected inverters with LCL filters," *IEEE Trans. Power Electron.*, vol. 31, no. 1, pp. 743–757, Jan. 2016.
[33] C. Chen, J. Xiong, Z. Wan, J. Lei, and K. Zhang, "A time delay compensation method based on area equivalence for active damping of an LCL -type converter," *IEEE Trans. Power Electron.*, vol. 32, no. 1, pp. 762–772, Jan. 2017.
[34] L. Corradini, W. Stefanutti, and P. Mattavelli, "Analysis of multisampled current control for active filters," *IEEE Trans. Ind. Appl.*, vol. 44, no. 6, pp. 1785–1794, Nov. 2008.
[35] C. Zhao, *Modeling and Simulation in the HVDC System*, 1st ed., vol. 1, Beijing, China: China Elect. Power Press, 2014, pp. 54–56.

Chuyang Wang received the B.E. degree in electrical engineering from Nanjing University of Aeronautics and Astronautics, Nanjing, China, in 2012, where he is currently working toward the Ph.D. degree at the Department of Electrical Engineering.

His research interests include modular multilevel converters, new energy power generation, and digital controls applied to power electronics.

Lan Xiao (M'06) was born in Zhejiang, China, in 1971. She received the B.S. and Ph.D. degrees in electrical engineering from Nanjing University of Aeronautics and Astronautics (NUAA), Nanjing, China, in 1993 and 1998, respectively.

In 1999, she joined the faculty of the College of Automation Engineering, NUAA, where she is currently a Professor with the Jiangsu Key Laboratory of New Energy Generation and Power Conversion. She has authored or coauthored more than 60 technical papers in journals and conferences. Her current research interests include soft-switching dc/dc converters, soft-switching inverters, and renewable energy generation systems.

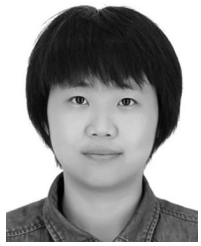

Huijie Jiang was born in Shanxi, China, in 1994. She received the B.E. degree and is currently working toward the M.S. degree in electrical engineering from Nanjing University of Aeronautics and Astronautics, Nanjing, Jiangsu.

Her research interests include power conversion, control of single-phase power rectifiers, and inverters.

Tingting Cai was born in Jiangsu, China, in 1994. She received the B.E. degree and is currently working toward the M.S. degree in electrical engineering from Nanjing University of Aeronautics and Astronautics, Nanjing, China.

Her research interests include power conversion, control of three-phase power rectifiers, and inverters.